Accepted Manuscript

Laser-induced SnS_2-SnS phase transition and surface modification in SnS_2 thin films

A. Voznyi, V. Kosyak, P. Onufrijevs, L. Grase, J. Vecstaudža, A. Opanasyuk, A. Medvid'

PII: S0925-8388(16)32136-3

DOI: 10.1016/j.jallcom.2016.07.103

Reference: JALCOM 38271

To appear in: *Journal of Alloys and Compounds*

Received Date: 24 April 2016

Accepted Date: 9 July 2016

Please cite this article as: A. Voznyi, V. Kosyak, P. Onufrijevs, L. Grase, J. Vecstaudža, A. Opanasyuk, A. Medvid', Laser-induced SnS_2-SnS phase transition and surface modification in SnS_2 thin films, *Journal of Alloys and Compounds* (2016), doi: 10.1016/j.jallcom.2016.07.103.

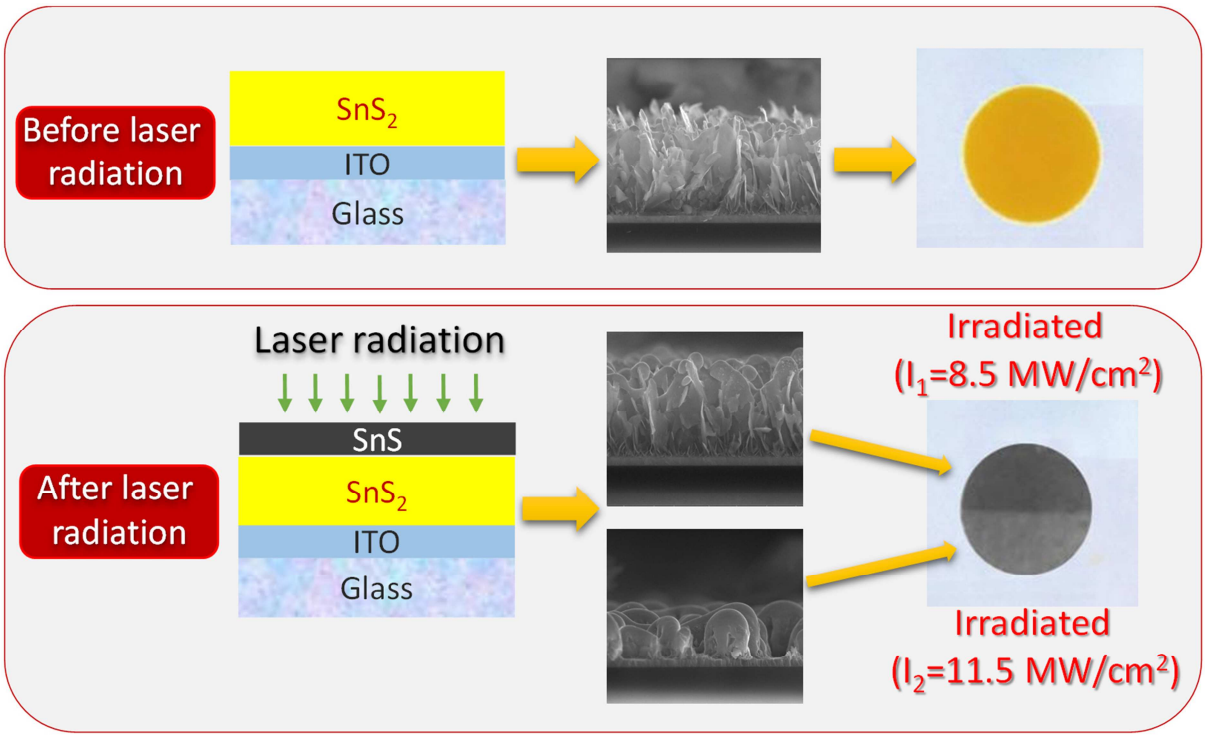

Laser-induced SnS_2-SnS phase transition and surface modification in SnS_2 thin films

A.Voznyi[1*], V.Kosyak[1], P. Onufrijevs[2], L.Grase[2], J. Vecstaudža[2],
A. Opanasyuk[1] and A. Medvid'[2]
[1]*Sumy State University, 2, Rymsky Korsakov Str., 40007 Sumy, Ukraine*
[2]*Riga Technical University, 3/7, Paula Valdena Str., LV-1048 Riga, Latvia*

Abstract

A thin film of SnS_2 obtained by close-spaced vacuum sublimation was irradiated by an Nd:YAG laser (λ=532 nm) using two intensities of laser radiation of 8.5 MW/cm^2 and 11.5 MW/cm^2. It was shown that laser irradiation leads to evaporation of sulphur from the surface, and the formation of SnS and Sn_2S_3 phases. The study of samples' cross-section by energy dispersive X-ray analysis reveals that in the case of irradiation at 8.5 MW/cm^2 intensity, the SnS layer is formed only at the surface of the initial SnS_2 thin film. The application of more intensive radiation of 11.5 MW/cm^2 leads to changes in chemical composition for the entire thin film. The formation of the predominant SnS phase, which includes a small amount of Sn_2S_3, was confirmed by the X-ray diffraction and Raman spectroscopy methods, as well as by measurements of optical reflectance and transmittance spectra. It was established that laser irradiation of the samples leads to the coalescence of grains accompanied by smoothing of the surface. The current-voltage characteristics of the ITO/Sn_xS_y/Al samples show an ohmic behaviour in the case of non-irradiated intensity samples; for irradiated samples, the diode behaviour of I-V curves was observed. This is considered as evidence of the formation of p-SnS/n-SnS_2 heterojunction by laser irradiation.

*Corresponding author: E-mail address: andrey.vozny@gmail.com (PhD student A. Voznyi)
Keywords: Tin sulphides; Thin films; Laser treatment; Phase transition; Phase composition.

1. Introduction

Sn_xS_y binary compounds have high potential use in optoelectronics. In particular, the SnS_2 compound with n-type conductivity has shown significant potential for photodetectors and for the window layer in solar cells due to high carrier mobility and the wide band gap that ranges between

2.24–2.6 eV, according to different sources [1–4]. The SnS p-type semiconductor exhibits unique properties for application in thin films solar cells as an absorber layer that can substitute for the widely used CdTe and CIGS [3,5]. This is because of a combination of being near the optimal band gap of 1.35 eV [3] and the high optical absorption coefficient [2]. Other important advantages of SnS-related compounds are their being low-cost, earth abundant and non-toxic [2]. The p and n-type conductivity of SnS and SnS_2 open the opportunity for the development of p-SnS/n-SnS_2 based solar cells [1,6]. A recent theoretical calculation reveals that the conversion efficiency of these solar cells is 25.3 % [7]. This correlates with the estimation performed earlier for the general case (e.g. single-junction solar cells), which shows that conversion efficiency of SnS based solar cells could be more than 24% [2,3]. On the other hand, the record efficiency of SnS based solar is only 4.4% [8]. The low efficiency is explained by the low homogeneity of the structure due to the formation of secondary phases and the presence of different types of defects. This requires the development of a method for growing high-quality Sn_xS_y layers. Several different methods are used for obtaining Sn_xS_y [3]. The close-spaced vacuum sublimation (CSS) method is widely used for deposition of high-quality compound semiconductor films [9–11]. However, this method has almost never been applied for the growth of Sn_xS_y films [12].

Laser technology is a powerful tool allowing improvement of crystal quality of bulk crystals or highly disordered polycrystalline films, as well as phase transition in compound semiconductors [13–18]. This makes it possible to overcome the limitation of solar cell efficiency due to recombination of free carriers on defect centres, or because of the presence of unfavourable secondary phases. However, laser irradiation is rarely used for Sn_xS_y compound processing [19].

For the Sn_xS_y compounds, controlling secondary phase formation is an important task, since SnS_2 could be transformed to SnS and vice versa by the changing of the concentration of volatile sulphur [2]. This is why films of Sn_xS_y compounds usually contain secondary phases [3]. The SnS_2-SnS phase transition has been studied only for thermal annealing [20]. At the same time, laser irradiation could be considered as an effective method for controllable phase transition in Sn_xS_y since it provides rapid increases of temperature in materials.

The specific crystal properties of SnS_2 are very sensitive to growth conditions and post-growth treatment. In particular, the SnS_2 compound is a layered material with a CdI_2-type structure, which consists of a sheet of Sn atoms between two sheets of hexagonally packed S atoms. The layered structure of SnS_2 is formed due to a combination of covalent and van der Waals bonding. Namely, atomic layers interact via the weak van der Waals force, while intralayer bonding is due to

the strong covalent force. SnS_2 can exist in a number of polytypes [21]. Therefore, structural analysis of SnS_2 films is complicated not only by the possible formation of Sn_2S_3 and SnS secondary phases, but also by the presence of different polytypes. It has been established that, in most cases, SnS_2 thin films have a hexagonal crystal structure of 2H polytype [12,22,23]. The influence of growth conditions on the crystal properties of SnS_2 films was studied in [12,22]. However, the effect of laser irradiation on crystal properties of SnS_2 has not yet been studied.

Thus, the aim of this paper is to study the effect of laser irradiation on SnS_2 in terms of phase transition, crystal structure and surface modification. In particular, the influence of laser irradiation on chemical composition, structural, optical and electrical properties were investigated.

2. Experimental

Similar to our previous work [24], SnS_2 thin films were obtained in a vacuum chamber VUP-5M by the CSS method. A detailed description and scheme of the device for producing the thin films is available in [9]. Samples were deposited on ultrasonically cleaned ITO (300 nm thickness) coated glass substrates. The stoichiometric powder of SnS_2 was used as an initial material for evaporation. The temperatures of the evaporator and substrate were 675 ^{0}C and 250 ^{0}C, respectively. The time of deposition was 4 min.

Laser irradiation of SnS_2 thin films samples was performed in air by the second harmonic of Nd:YAG laser (λ=532 nm). The samples were irradiated with two different intensities of laser radiation, namely I_1=8.5 MW/cm^2 and I_2=11.5 MW/cm^2. The focused laser beam (spot diameter of 1.5×10^{-3} and 1.3×10^{-3} m for I_1 and I_2 intensities, respectively) was scanned over the sample surface at a constant speed of 1.6×10^{-4} m/s; the duration of the impulse was 4 ns. The scanned area was 0.56×10^{-4} m^2 for both I_1 and I_2 intensities.

The surface morphology and chemical composition of the thin films were investigated using FEI Nova NanoSEM 650 Schottky field emission scanning electron microscope (FESEM) with an integrated Apollo X energy dispersive spectroscope (EDS) for the chemical composition analysis using standardless energy techniques. The following parameters of the EDS experiment were used: accelerating voltage 15 kV, detector resolution 125.4 eV, working distance 7 mm and spot size 5.5. The calculation of the concentrations was determined by averaging results of at least 10 measurements from different points on the surface. The thickness was measured by FESEM directly from the cross-section of the samples.

Also, to study the microstructure of the surface and to estimate its roughness, the NT-MDT atomic force microscope (AFM) in semi-contact mode was used.

Structural analysis was carried using Rigaku Ultima+ X-ray diffractometer (XRD) operating in Bragg-Brentano geometry using KαCu radiation source. The scan step was 0.05 2θ degrees, and the range was variable from 10–80^0 2θ degrees. Identification of the crystal phases was performed with the Crystallography Open Database (COD).

Room temperature Raman spectroscopy (RS) spectra were studied using Renishaw InVia90V727 micro-Raman spectrometer in a backscattering geometry using 1200 and 1800 mm^{-1} grating for the semiconductor infrared (λ=785 nm) and Ar green (λ=514nm) laser excitation, respectively. Recording the signal was carried out by a CCD camera. Calibration of the spectrometer was performed by measuring the 520 cm^{-1} Raman line of the silicon wafer. For the measurements, the power of excitation and exposure time was set in such a way as to obtain sufficient signal-to-noise ratio of the spectra without damaging the surface due to local overheating.

In order to evaluate optical band gap of the materials reflectance and transmittance spectra were measured using Solid Spec-3700 UV-VIS-NIR Shimadzu Spectrophotometer.

The measurements of the dark and light current-voltage (I-V) characteristics of the ITO/Sn_xS_y/Al sandwich structures were carried out using Keithley M 6487 pico-amperemeter. The Al contacts were deposited by thermal vacuum evaporation on the surface of as-grown samples and immediately after laser irradiation, at a substrate temperature of 100 ^{0}C.

3. Results and discussion

3.1. Surface morphology and chemical composition

The change in colour of the samples after irradiation was visually observed. Namely, the colour of the surface irradiated with the intensity of I_1 changed from yellow, typical for SnS_2 [2], to a dark grey SnS-like colour, which is the evidence of sulphur evaporation and phase transition from SnS_2 to SnS. As well as for the previous regime of laser irradiation, the colour of the surface irradiated with the intensity of I_2 changed to grey. However, the colour of the irradiated surface was lighter.

The FESEM image of the surface of the non-irradiated SnS_2 film is shown in Fig. 1(a). As can be seen, the thin films consist of plate-like crystallites randomly oriented in a plane parallel to the surface. The higher magnification FESEM image (Fig. 1(a), insert) shows that the length of

crystallites is about 1 µm, and their thickness is less than 100 nm. It should be noted that the surface of the thin film is homogeneous, i.e. free of any large-scale defects and precipitates. The plate-like structure of the crystallites is clearly visible on the FESEM cross-sectional image presented in Fig. 1(b). Also, it can be seen that the crystallites are well oriented along a plane perpendicular to the surface. The thickness of the films is about 4.1 µm.

The irradiation of the surface with the intensity of I_1 leads to agglomeration and coalescence of grains and formation of islands with 1 µm length (Fig. 1(c)). As can be seen from Fig. 1(c) (insert), the surface of the islands is rather homogeneous and does not contain any defects such as cracks, holes or voids. It should be noted that the cross-sectional FESEM image (Fig. 1(d)) clearly shows that the surface after laser irradiation is smooth, and the shape of the crystallites became rounder. Also, the thickness of the samples decreased to 3.6 µm due to evaporation of material.

Application of more intensive laser irradiation of I_2 leads to further enlargement of islands due to agglomeration, and the distance between the islands on the surface is increased. As follows from Fig. 1(e), the average length of islands varies from 1 µm (in this case they have a circular shape: Fig. 1(e), inset), to 5 µm for oblong islands. The cross-sectional view (Fig. 1(f)) shows that crystallites coalesced to form drop-like islands with an average height of 2.8 µm.

The AFM study of the samples allows us to determine more accurately the size of the grains and surface roughness; the AFM scans and height profiles are presented in Fig. 2. In particular, as follows from Fig. 2(a), the average thickness and length of the plate-like crystallites of the nonirradiated sample is 1 and 2 µm, respectively. Moreover, using the height profile, it was found that the thickness of plate-like crystallites decreases with height to about 0.1 µm at the top of the crystallites. Thus, it can be concluded that the crystallites have a cone-like profile. The roughness of the non-irradiated sample is about 0.7 µm.

Comparing Fig. 2(a) and Fig. 2(b), it was found that during the irradiation with the intensity of I_1 the sharp crystallites coalesced into larger smooth cone-like islands. The average diameter of such cones is more than 2 µm near the base and 0.5 µm at the top. The distance between cones is about 2.4 µm. The roughness of the irradiated surface is about 0.6µm (Fig. 2(b)). Under more intensive laser irradiation with the intensity of I_2 the diameter of islands increased to 2.5 µm near the base and 1.5 µm at the top (Fig. 2(c)). The AFM scan (Fig. 2(c)) confirms the results of the FESEM study (Fig. 1(e)): the distance between islands increases to about 3.5 µm with increasing irradiation intensity. Also, the roughness of the surface is close to the height of islands of about 3 µm observed on the cross-sectional FESEM image (Fig. 1(f)). Thus, it was found that the surface of the sample consists of

free-standing drop-like crystallites, which are formed due to melting and agglomeration of crystallites.

The stoichiometric composition of SnS_2 was reported to be δ=0.46 [2] and δ=0.5 [25] (where δ=[Sn]/[S] (at.%)). However in [23,26], the EDS analysis shows more Sn-rich composition of about δ=0.54, whereas XRD and Raman methods reveal the single-phase structure of the samples. In our study the EDS analysis of the surface of non-irradiated samples shows a Sn-rich chemical composition, namely the value of δ is 0.57 (Fig. 1(a) inset). This can be explained by the re-evaporation sulphur during deposition. The scan of the surface reveals concentration uniformity. A small variation of the chemical composition on the cross-section was observed. In particular, as follows from Fig. 1(b), the Sn concentration decreases with depth to δ=0.52 (at the middle of sample cross-section), and slightly increases again to δ=0.54. The layer at the substrate shows the highest Sn composition of δ=0.61. We speculate that this could be due to the interaction of the EDS beam with Sn contained ITO coating.

The EDS analysis of sample irradiated with the intensity of I_1 (dark grey surface) confirms our assumption that changes in colour from initial yellow to dark grey are due to evaporation of sulphur from the surface. The surface composition of the irradiated sample is δ=0.72 (Fig. 1(c)). The EDS analysis of the cross-section (Fig. 1(d)) shows that the thickness of the layer with δ=0.72 composition is about 1 μm. The chemical composition directly next to this layer was δ=0.61, which is more Sn-rich than the composition of the nonirradiated sample at the same depth. The chemical composition at the middle of sample's cross-section and at the substrate is similar to that in the nonirradiated sample. This reflects that the depth of the impact of laser irradiation with the intensity of I_1 is about 2 μm.

EDS analysis of surface irradiated with the intensity of I_2 (light grey surface) shows that increasing laser intensity leads to more intensive evaporation of sulphur, hence enrichment of the surface with metal. The surface chemical composition was found to be δ=0.87 (Fig. 1(e)). Also, as follows from Fig. 1(f), the sulphur loss takes place throughout the depth of the sample. In particular, the concentration of Sn monotonically decreases with depth increasing from δ=0.87 on the surface to δ=0.72 at the substrate. Thus, the gradient in Sn concentration due to the decreased influence of laser irradiation with depth was formed.

It should be noted that the accuracy of EDS measurements of rough surfaces could be is only of 5 at.% [27]. Nevertheless, the obtained EDS results are sufficiently reliable to determine a general trend in the effect of laser irradiation on the chemical composition of the samples.

3.2 Structural analysis

In order to avoid misinterpretation of XRD results due to overlapping of Sn_xS_y and ITO-related reflection, XRD measurements of ITO-coated glass substrate were carried out. As can be seen from Fig. 3(a), the XRD pattern shows diffraction lines typical for ITO [28,29].

The XRD patterns of the non-irradiated and irradiated samples are presented in Fig. 3. As follows from Fig. 3(b), the non-irradiated sample is single-phase hexagonal SnS_2. In particular, reflections from (001), (100), (101), (110) and (111) planes at 15^0, 28.4^0, 32.2^0, 50^0, 52.6^0 respectively, of hexagonal 2H-SnS_2 were detected [21]. The calculated values of the lattice parameter were as follows: a =0.3646 nm and c =0.5859 nm. The value of a and c is in good agreement with reference data [30].

The irradiation of the sample with the intensity of I_1 strongly affected the phase composition of the films. Namely the (111) SnS-related line at 31.8^0 [31] is clearly visible on the shoulder of the (101) line of the SnS_2 phase . Also weak peaks at 16.2^0 and 26.6^0, which correspond to reflections from (120) and (111) respectively of the Sn_2S_3 phase [32], were detected (Fig. 3(c)). Taking into account the results of the EDS analysis of the cross-section of the irradiated sample, it can be concluded that the SnS and Sn_2S_3 phases are mostly located at the surface layer.

For the sample irradiated with the intensity of I_2 the increasing intensity of the (111) SnS-related line as well as the (120) and (111) Sn_2S_3-related lines indicates the increasing concentration of these phases (Fig. 3(d)). Moreover, the highest intensity of the SnS-related (111) line at 31.8^0 shows that the SnS phase is dominant over the SnS_2 and Sn_2S_3 phases.

3.3 Raman analysis

In order to identify SnS_2, Sn_2S_3 and SnS-related modes on Raman spectra, we used reference data about their frequencies in single crystals [33–36]. However, Raman analysis of polycrystalline thin films can be complicated by shifting and broadening of the peaks compared to those in single crystals due to grain boundaries, extended defects and stresses [37–40].

For reliable Raman phase analysis of the Sn_xS_y compounds, the energy of excitation should be close to the band gap of the studied phase. In this case, one can expect high absorption of excitation radiation or even resonance conditions [41], and hence high signal to noise ratio of the Raman spectra. Taking into account the difference between the band gap energies of SnS_2, Sn_2S_3 and SnS_2

compounds, we used two wavelengths of excitation. Namely, for identification of SnS_2 phase, excitation with a 514 nm green laser is optimal, since the energy of excitation (E=2.41 eV) is close to the band gap of SnS_2 (E_g=2.24 eV). For the identification of Sn_2S_3 and SnS_2 phases with the band gaps of (E_g=1.09 eV) and (E_g=1.35 eV), the 785 nm IR excitation (E =1.58 eV) is more suitable.

The Raman spectra measured with 514 nm excitation are presented in Fig. 4. The sufficiently good-quality spectra with a large signal-to-noise ratio of the non-irradiated sample (Fig. 4) were obtained with an exposure time of 120 s, and laser excitation power density of 33.89 W/cm^2. Increasing the exposure time to 200 s did not lead to significant changes in the quality of the spectra and intensities of peaks. It should be noted that, in order to prevent sample damage due to overheating, the excitation power density did not exceed 33.89 W/cm^2.

As can be seen from Fig. 4(a), the Raman spectrum of the non-irradiated sample shows a high-intensity peak at 314.7 cm^{-1}. This peak could be assigned with A_{1g} optical phonon mode of 2H-SnS_2 polytype with hexagonal symmetry which is related to Sn-S bonding in the a-c plane [36,42,43]. The frequencies of the observed peaks and their possible interpretations are listed in Table 1. The 2H-SnS_2 polytype structure implies the presence of weak E_g mode at 205 cm^{-1} along with a strong A_{1g} mode (Table 1) [36]. However, the E_g mode was not clearly detected. We observed only very small increases of intensity at around 204 cm^{-1} (Fig. 4(a)). The absence of other modes on Raman spectra confirms the single-phase hexagonal structure of the non-irradiated SnS_2 sample. It should be noted that this finding is consistent with the results of XRD analysis.

As can be seen from Fig. 4(b), the irradiation of the samples with the intensity of I_1 leads to the appearance of an additional three broad weak peaks centered at 92, 189 and 227 cm^{-1}. Taking into account the results of EDS and XRD studies for the irradiated, sample we assumed that these peaks are related to the SnS and SnS_2 phases. According to selection rules [33], the presence and frequencies of Raman modes depend on the orientation of the crystal lattice with respect to the direction of the incident and scattered photons. As was shown elsewhere [33,35] for most cases, the A_g mode related to bonding in the a-c plane is dominant for both SnS and Sn_2S_3 phases. Also, in some cases of orientation crystal lattice, the less intensive B_{1g}, B_{2g} and B_{3g} modes could be observed (Table 1) [33,35]. Moreover, in the case of Sn_2S_3 only the A_g mode has been observed experimentally [34,44]. As can be seen from Fig. 4(c), the peak at 92 cm^{-1} consists of two overlapping peaks at 88 cm^{-1} and 95 cm^{-1} related to the A_g mode of the Sn_2S_3 and SnS phases, respectively. The broad weak peak at 189 cm^{-1} also could be assigned to A_g mode of the SnS phase (Table 1). We speculate that another broad weak peak centered at 227 cm^{-1} is related to two close A_g modes of SnS and Sn_2S_3 at

around 220 and 236 cm^{-1} respectively (Table 1). However, it is difficult to distinguish the exact position of the peaks. It should be noted that A_g mode of Sn_2S_3 mode at 308 cm^{-1} was not observed on the spectrum, probably due to overlapping with the broad A_{1g} mode of the SnS_2 phase at 314.7 cm^{-1}.

As was shown by XRD and EDS analysis, the irradiation of the sample with the higher intensity of I_2 results in increasing the concentration of the SnS and Sn_2S_3 phases. This finding was confirmed by Raman spectroscopy. The relative intensity of the SnS and Sn_2S_3-related modes is significantly increased, while the intensity of the A_{1g} mode of the SnS_2 phase is decreased (Fig. 4 (c)). Here, the SnS- related A_g mode is dominant. Moreover, one more SnS- related B_{3g} mode at 162 cm^{-1} was observed.

The Raman spectra measured with IR 785 nm excitation are presented in Fig. 5. The good quality spectra of the non-irradiated sample (Fig. 5(a)) were obtained with a short exposure time of 30 s and laser excitation power density of 2.22 W/cm^2. It was found that, in contrast to measurements of irradiated samples with green laser excitation, the increasing of the exposure time (in this case from 10 to 30 s) led to a significant improvement of the quality of the Raman spectra, as well as increasing the relative intensity of SnS- and Sn_2S_3-related modes (Fig. 5(b, c)). Thus, the spectra measured with an exposure time of 30 s were analysed.

Application of IR excitation radiation for Raman analysis of the non-irradiated SnS_2 sample gives very similar results to those obtained with a green laser. In particular, as follows from Fig. 5(a), the Raman spectrum of the non-irradiated sample shows one strong SnS_2-related A_{1g} mode at 314.5 cm^{-1}. In general, the spectrum measured with IR excitation for irradiated samples confirms the results obtained with green wavelength excitation. Namely, the trend of increasing relative intensities of SnS- and Sn_2S_3-related modes compared to the A_{1g} mode of SnS_2 with the intensity of laser irradiation was observed. However, in contrast to the Raman spectra measured with green excitation, the spectra obtained with IR excitation show strong SnS- and Sn_2S_3-related modes, even for the sample irradiated with the intensity of I_1. In particular, the SnS-related A_g mode at around 221cm^{-1} is dominant on both spectra of samples irradiated with the intensities of I_1 and I_2. As was discussed above, this can be explained by the fact that relatively narrow band gap SnS and Sn_2S_3 compounds interact much stronger with IR than green wavelength radiation. As a result, three peaks of the SnS-related A_g mode at 95, 184 and 221 cm^{-1} and a peak that could be assigned to the B_{2g} mode at 288 cm^{-1} (as well as three peaks of the Sn_2S_3-related A_g mode at 88, 154 and 309 cm^{-1}) are clearly observed.

In order to study the spatial distribution of phases, micro-Raman mapping using IR excitation of the non-irradiated and irradiated surfaces was performed. For comparing with the irradiated

surface, one side of the sample was left non-irradiated. On the other side, two rectangular areas were irradiated by a laser with intensities of I_1 and I_2. As a result, three areas close to each other were formed on a surface of the samples (Fig. 6(a, b)). These areas were visually distinguishable since they had a different colour. The non-irradiated area was yellow, and analogous to fully irradiated samples, the areas irradiated by a laser with the intensities of I_1 and I_2 were grey and light-grey, respectively. The edges of the irradiated areas were not sharp, and the narrow intermediate zones between irradiated areas with mixed yellow-grey or grey-light grey colours were observed (Fig. 6(a,b)). This can be explained by the non-uniform power density of the laser spot. The overlapping of laser spots during step-by-step scanning provides a uniform distribution of power density of laser irradiation. Thus, the non-uniformity of the laser spot manifested itself only at the edges of the scanned area.

The measurement parameters for each spectrum of micro-Raman mapping power were as follows: density of laser excitation 0.05, and exposure time 10 s. Thus, the mapping spectra were similar to the single scan spectrum measured with an exposure time of 30 s (Fig. 5(b, c)). The scanned area includes non-irradiated and irradiated with the intensity of I_1 surfaces, or surfaces irradiated with the intensities of I_1 and I_2, as shown on Fig. 6(a, b). This allows the effect of laser irradiation on the surface distribution of phases to be compared. As a parameter of study, the ratio of peak intensities ($R=I(SnS_2)/I(SnS)$) of SnS_2-related A_{1g} mode at about 314.5 cm^{-1} and SnS-related A_g mode at about 95 cm^{-1} was used.

As can be seen from Fig. 6(a), the value of R for the non-irradiated yellow coloured surface is about 10. Basically, this corresponds to the ratio of the intensity of A_{1g} to the intensity of the background. This means that no peak of SnS-related A_g mode at about 95 cm^{-1} was detected. Thus, the non-irradiated yellow coloured area corresponds to single phase SnS_2. The value of R decreases for the intermediate zone between the non-irradiated and irradiated areas, which indicates the appearance of the SnS-related A_g mode. This mode became more pronounced for the irradiated area. The intensity of the SnS_2-related A_{1g} mode is only two times higher than that of the SnS-related A_g mode (R=2). It should be noted that the surface distribution of R values for the irradiated surface is rather uniform. This reveals the homogeneous surface distribution of the SnS and SnS_2 phases.

The R value for the surface irradiated with the intensity of I_2 is about 1 or less. This indicates the dominance of the SnS phase. Also, mapping shows a non-uniform distribution of R. Namely, the value of R is varied across the surface from 0.8 to 1. This can be explained by the non-homogeneous surface distribution of the SnS and SnS_2 phases. On the other hand, taking in account that absorption of laser excitation depends not only on phase composition but also on the properties of the surface,

the non-uniform distribution of R could be due to the high roughness of the surface formed by drop-like islands.

3.5. Optical properties

The reflectance and transmittance spectra of the samples are presented in Fig. 7 (a,b). It should be noted that the minimum at about 1100 nm was observed on the transmittance spectrum of the SnS_2 films deposited on ITO-coated glass substrate (Fig. 7a). It was assumed that this minimum is due to the presence of the ITO layer. Thus, in order to avoid the effect of ITO coating on optical spectra of non-irradiated SnS_2 and irradiated samples, we used thin films obtained on a glass substrate. These samples were deposited and irradiated under the same conditions as those that were previously obtained on ITO-coated glass. As was expected, the minimum at 1100 nm was not observed on the transmittance spectrum of the glass/SnS_2sample and hence, in contrast to samples obtained on the ITO-coated glass, there is only one clearly distinguishable transmission edge at about 500 nm. Therefore, for further optical characterisation, only the samples obtained on glass substrate were used. It should be noted that both SnS_2 samples deposited on glass and ITO-coated glass showed this transmission edge, indicating reproducibility in optical properties of the samples obtained by the CSS method.

As can be seen from Fig. 7, the laser irradiation has a strong influence on the optical properties of the films. In particular, the transmittance of the irradiated samples decreases by about 20% and 30% for samples irradiated with the intensities of I_1 and I_2, respectively. The transmittance edge E_{t1} shifts from 2.48 eV for non-irradiated samples to E_{t2}=1.72 eV and E_{t4}=1.59 eV for samples irradiated with the intensities of I_1 and I_2, respectively. It is important to note that an additional short-wavelength transmission edge at about E_{t3}=2.72 eV is observed in the transmittance spectra of the sample irradiated with the intensity of I_1. This transmission edge could be associated with a bottom SnS_2 layer of the SnS_2/SnS two-layer structure formed after laser irradiation.

A similar effect of the laser irradiation was observed for reflection spectra. Namely, the reflectance of the irradiated samples drops and the optical reflectance edge E_{r1} shifts from 2.48 eV for non-irradiated samples to E_{r2}=1.8 eV and E_{r3}=1.72 eV for samples irradiated with the intensities of I_1 and I_2, respectively. The shift of transmittance and reflectance edges can be explained by a phase transition from SnS_2 to SnS. The decrease of reflectance and transmittance is not only due to phase transition accompanied by changes in transmittance and reflectance coefficient, but also to the

modification of the surface after the irradiation. In particular, we speculate that the light scattering on platelet-like grains of the non-irradiated samples could be considerably different to that on drop-like islands observed on the surface of the irradiated samples.

For the reliable determination of the band gap energies, the absorption coefficient was calculated using reflectance and transmittance spectra. Then, the direct and indirect energy gaps were determined by plotting the $(\alpha h\nu)^2$ and $(\alpha h\nu)^{\frac{1}{2}}$, respectively, as a function of the photon energy $h\nu$, as shown in Fig. 8. As follows from Fig. 8(a), the direct and indirect band gaps of the non-irradiated SnS_2 sample were found to be 2.70 eV and 2.62 eV, respectively. The value of the direct band gap is in good correlation with results of theoretical calculations reported in [4], but it is higher than values of about 2.2–2.5 eV obtained in [23,45–47] for SnS_2 thin films. The relatively broad band gap of the SnS_2 sample could be due to the quantum size effect, since the FESEM and AFM studies show that the thickness of platelet-like grains at the surface is less than 100 nm. For example, the significant increase of the band gap of SnS_2 due to the quantum size effect was observed for nanostructured thin films in [26,48].

The direct band gap of films irradiated with the intensities of I_1 and I_2 was found to be 2.33 eV and 2.04 eV, respectively, and the indirect band gap 2.16 eV and 1.67 eV, respectively (Fig. 8(b,c)). Taking into the account the multi-phase composition of the samples irradiated with the intensities of I_1 and I_2, it is difficult to associate unambiguously the obtained energies with one of the phases. However, the decreases of the optical band gap with the intensity of the laser irradiation are obvious. This corresponds to the evaporation of sulphur from initial pure SnS_2 films and the appearance of the Sn_2S_3 or SnS phases.

3.5. Electrical properties

The main aim of the I-V measurements is to study the possibility of the formation of the n-SnS_2/p-SnS junction after laser irradiation. Thus, in order to avoid the formation of Schottky barriers and hence misinterpretation of the results of the I-V measurements, it is necessary to obtain ohmic contacts for the samples.

The electron affinity of SnS_2 is 4.2 eV [2,49], and it is difficult to obtain the ohmic contact for n-SnS_2, since the work function (ϕ_M) of the most commonly used metals is more than 4.2 eV. Taking this into account, Al with ϕ_M of about 4.2 eV could be considered as one of the best candidates for

ohmic contact ton-SnS_2. For example, the Al contacts were found to be ohmic for n-SnS_2 crystals in [50,51]. Also, Al is suitable for formation of the ohmic contact with p-SnS [1,52].

It should be noted that metal-semiconductor barriers could be reduced due to the presence of surface states, which are typical for highly disordered polycrystalline material, or with the doping of semiconductor. In the case of doping, the width of the depletion region decreases, and the charge carriers can tunnel through the depletion region [53]. With this purpose, in order to provide diffusion of Al into the sample and hence doping at the surface of as-grown and irradiated samples, the deposition of contact was performed under a substrate temperature of 100 ^{0}C.

The I-V curves measured for non-irradiated SnS_2 and irradiated with the intensities of I_1 and I_2 samples are shown in Fig. 9. As can be seen, the I-V curve of ITO/SnS_2/Al sample is linear (ohmic). This means that there are no electrical barriers between SnS_2 and Al, or ITO contacts were found. The dark conductivity of the sample was 7.7×10^{-4} $\Omega^{-1}\cdot cm^{-1}$. This value is in a good agreement with the results obtained in [45,54,55].0 -7 ~-1

The I-V curve of the sample irradiated with the intensity of I_1 shows typical diode behaviour. On the other hand, for the I-V curve of the sample irradiated with the intensity of I_2, the current rectification was much less pronounced. In particular, the degree of current rectification calculated as the ratio of currents at +0.5 and -0.5 V for the samples irradiated with the intensities of I_1 and I_2 is 13 and 2, respectively. Taking into account the results of EDS analysis of the samples' cross-sections, it can be concluded that in the case of laser irradiation with the intensity of I_1, the two-layer n-SnS_2/p-SnS junction was formed, which is reflected in the diode behaviour of the I-V curve. The application of higher intensity laser irradiation of I_2 leads to the formation of a mixture of SnS and SnS_2 phases, rather than a two-layer structure with a sufficiently sharp boundary between the layers.

4. Conclusions

It was shown that laser irradiation of the SnS_2 films provides evaporation of sulphur and hence phase transition to the SnS and Sn_2S_3 phases. The depth phase distribution in irradiated samples is strongly dependent on the intensity of the laser radiation. In particular, the irradiation of the samples with intensity of I_1=8.5 MW/cm^2 leads to the formation of the SnS layer at the surface. This results in the formation of two-layer SnS/SnS_2 structure. Also, irradiated films contain a small amount of the Sn_2S_3 phase. We speculate that this phase is located between the SnS and SnS_2 layers since the Sn to S ratio concentration monotonically decreases with depth. The application of a more intensive irradiation with the intensity of I_2=11.5 MW/cm^2 leads to changes in chemical composition

for whole thin films and the formation of a mixed-phase layer with a predominance of the SnS phase over the SnS_2 and Sn_2S_3 phases. The clearly distinguishable phase separation (i.e. multilayer structure) was not found.

Thus, it has been established that laser irradiation could be effectively used for modification of chemical and phase composition of Sn_xS_y thin films. In our opinion, this opens new possibilities for improvement of Sn_xS_y-based optoelectronic devices. For example, the evaporation of sulphur under laser radiation may lead to the formation of the thin Sn-rich layer at the surface of the SnS film. Such a metal-rich layer could have properties similar to highly-doped semiconductors. In turn, this allows metal-semiconductor barriers to be avoided between the absorber layer and the top metal contact. Highly doped semiconductors usually form ohmic contacts with most metals, even with those metals having a high work function. In the best case scenario, the Sn metal contact could be formed on the surface of SnS by the laser-induced evaporation of the sulphur. Also, the smoothing of the surface observed here due to the melting accompanied by the agglomeration of the grains into the islands could lead to increasing of the area of contact between layers, and suppression of the grain boundaries' recombination.

The possibility of the formation of the n-SnS_2/p-SnS heterojunction using laser irradiation of SnS_2 thin film requires additional careful experimental study. However, preliminary results obtained in here are promising, as the diode behaviour of the current-voltage dependencies of the irradiated samples was observed. Further improvement of the performance of n-SnS_2/p-SnS heterojunctions formed by laser irradiation could be achieved by the interplay between thicknesses of the initial SnS_2 thin film and the conditions of laser annealing.

Acknowledgments

This work was supported by the Ministry of Education and Science of Ukraine (Grant # 0115U000665c). A. Voznyi and Dr.V. Kosyak acknowledges Erasmus Mundus Ianus II program.

References

[1] A. Sánchez-Juárez, A. Tiburcio-Silver, A. Ortiz, Fabrication of SnS_2/SnS heterojunction thin film diodes by plasma-enhanced chemical vapor deposition, Thin Solid Films, 480-481 (2005) 452–456. doi:10.1016/j.tsf.2004.11.012.

[2] L.A. Burton, D. Colombara, R.D. Abellon, F.C. Grozema, L.M. Peter, T.J. Savenije, G. Dennler, A. Walsh, Synthesis, Characterization, and Electronic Structure of Single-Crystal SnS, Sn_2S_3 , and SnS_2, Chem. Mater. 25 (2013) 4908–4916. doi:10.1021/cm403046m.

[3] J.A. Andrade-Arvizu, M. Courel-Piedrahita, O. Vigil-Galán, SnS-based thin film solar cells: perspectives over the last 25 years, J. Mater. Sci. Mater. Electron. 26 (2015) 4541–4556. doi:10.1007/s10854-015-3050-z.

[4] L.A. Burton, T. Whittles, D. Hesp, W.M. Linhart, J.M. Skelton, B. Hou, R.F. Webster, G. O'Dowd, C. Reece, D. Cherns, D.J. Fermin, T.D. Veal, V.R. Dhanak, A. Walsh, Electronic and optical properties of single crystal SnS_2: an earth-abundant disulfide photocatalyst, J. Mater. Chem. A. 4 (2015) 1312–1318. doi:10.1039/C5TA08214E.

[5] S. Prasert, Development of Earth-Abundant Tin (II) Sulfide Thin-Film Solar Cells by Vapor Deposition, 2013.

[6] J.-H. Ahn, M.-J. Lee, H. Heo, J.H. Sung, K. Kim, H. Hwang, M.H. Jo, Deterministic Two-Dimensional Polymorphism Growth of Hexagonal n-Type SnS_2 and Orthorhombic p-Type SnS Crystals, Nano Lett. 15 (2015) 3703–8. doi:10.1021/acs.nanolett.5b00079.

[7] S. Lin, X. Li, H. Pan, H. Chen, X. Li, Y. Li, Numerical analysis of SnS homojunction solar cell, Superlattices Microstruct. 91 (2016) 375–382. doi:10.1016/j.spmi.2016.01.037.

[8] P. Sinsermsuksakul, L. Sun, S.W. Lee, H.H. Park, S.B. Kim, C. Yang, et al., Overcoming Efficiency Limitations of SnS-Based Solar Cells, Adv. Energy Mater. 4 (2014) 1400496. doi:10.1002/aenm.201400496.

[9] V. Kosyak, A. Opanasyuk, P.M. Bukivskij, Y.P. Gnatenko, Study of the structural and photoluminescence properties of CdTe polycrystalline films deposited by close-spaced vacuum sublimation, J. Cryst. Growth. 312 (2010) 1726–1730. doi:10.1016/j.jcrysgro.2010.02.034.

[10] Y.P. Gnatenko, P.M. Bukivskij, A.S. Opanasyuk, D.I. Kurbatov, M.M. Kolesnyk, V.V. Kosyak, H. Khlyap, Low-temperature photoluminescence of II–VI films obtained by close-spaced vacuum sublimation, J. Lumin. 132 (2012) 2885–2888. doi:10.1016/j.jlumin.2012.06.003.

[11] D. Kurbatov, V. Kosyak, M. Kolesnyk, A. Opanasyuk, S. Danilchenko, Morfological and structural characteristics of II-VI semiconductor thin films (ZnTe, CdTe, ZnS), Integr. Ferroelectr. 103 (2010) 32–40. http://www.tandfonline.com/doi/abs/10.1080/10584580802558126 (accessed May 29, 2015).

[12] C. Shi, P. Yang, M. Yao, X. Dai, Z. Chen, Preparation of SnS_2 thin films by close-spaced sublimation at different source temperatures, Thin Solid Films. 534 (2013) 28–31. doi:10.1016/j.tsf.2013.01.072.

[13] H.J. Meadows, A. Bhatia, V. Depredurand, J. Guillot, D. Regesch, A. Malyeyev, D. Colombara, M.A. Scarpulla, S. Siebentritt, P.J. Dale, Single Second Laser Annealed $CuInSe_2$ Semiconductors from Electrodeposited Precursors as Absorber Layers for Solar Cells, J. Phys. Chem. C. 118 (2014) 1451–1460. doi:10.1021/jp409804s.

[14] A. Bhatia, H. Meadows, A. Crossay, P.J. Dale, M.A. Scarpulla, Continuous wave solid phase laser annealing of single-pot electrodeposited $CuInSe_2$ thin films: Effects of Cu/In stoichiometry, J. Appl. Phys. 114 (2013) 044904. doi:10.1063/1.4816250.

[15] B.J. Simonds, H.J. Meadows, S. Misra, C. Ferekides, P.J. Dale, M.A. Scarpulla, Laser

processing for thin film chalcogenide photovoltaics: a review and prospectus, J. Photonics Energy. 5 (2015) 050999. doi:10.1117/1.JPE.5.050999.
[16] R. Kitagawa, H. Takebe, K. Morinaga, Photoinduced phase transition of metallic SmS thin films by a femtosecond laser, Appl. Phys. Lett. 82 (2003) 3641. doi:10.1063/1.1577824.
[17] A. Mychko, A. Medvid, E. Dauksta, Laser-induced increase of resistivity and improvement of optical properties of CdZnTe crystal, J. Cryst. Growth. 415 (2015) 47–50. doi:10.1016/j.jcrysgro.2014.12.028.
[18] A. Medvids, P. Onufrijevs, E. Dauksta, N.A. Sobolev, Homo- and Hetero-Structure Formation in Semiconductors by Laser Radiation: First Stage of Quantum Cones Formation, Solid State Phenom. 205-206 (2013) 475–479. doi:10.4028/www.scientific.net/SSP.205-206.475.
[19] D. Avellaneda, B. Krishnan, T.K. Das Roy, G.A. Castillo, S. Shaji, Modification of structure, morphology and physical properties of tin sulfide thin films by pulsed laser irradiation, Appl. Phys. A. 110 (2012) 667–672. doi:10.1007/s00339-012-7148-3.
[20] M.G. Sousa, A.F. da Cunha, P.A. Fernandes, Annealing of RF-magnetron sputtered SnS_2 precursors as a new route for single phase SnS thin films, J. Alloys Compd. 592 (2014) 80–85. doi:10.1016/j.jallcom.2013.12.200.
[21] C.R. Whitehouse, A.A. Balchin, Polytypism in tin disulphide, J. Cryst. Growth. 47 (1979) 203–212. doi:10.1016/0022-0248(79)90243-4.
[22] L. Amalraj, C. Sanjeeviraja, M. Jayachandran, Spray pyrolysised tin disulphide thin film and characterisation, J. Cryst. Growth. 234 (2002) 683–689. doi:10.1016/S0022-0248(01)01756-0.
[23] N.G. Deshpande, A.A. Sagade, Y.G. Gudage, C.D. Lokhande, R. Sharma, Growth and characterization of tin disulfide (SnS_2) thin film deposited by successive ionic layer adsorption and reaction (SILAR) technique, J. Alloys Compd. 436 (2007) 421–426. doi:10.1016/j.jallcom.2006.12.108.
[24] A. Voznyi, V. Kosyak, A. Opanasyuk, N. Tirkusova, L. Grase, A. Medvids G. Mezinskis, Structural and electrical properties of SnS_2 thin films, Mater. Chem. Phys. 173 (2016) 52–61. doi:10.1016/j.matchemphys.2016.01.036.
[25] R.C. Sharma, Y.A. Chang, The S−Sn (Sulfur-Tin) system, Bull. Alloy Phase Diagrams. 7 (1986) 269–273. doi:10.1007/BF02869004.
[26] S.K. Panda, a. Antonakos, E. Liarokapis, S. Bhattacharya, S. Chaudhuri, Optical properties of nanocrystalline SnS_2 thin films, Mater. Res. Bull. 42 (2007) 576–583. doi:10.1016/j.materresbull.2006.06.028.
[27] J. Goldstein, D.E. Newbury, D.C. Joy, C.E. Lyman, P. Echlin, E. Lifshin, L. Sawyer, J.R. Michael, Scanning Electron Microscopy and X-ray Microanalysis: Third Edition, Springer Science & Business Media, 2012. https://books.google.com/books?id=wq7eBwAAQBAJ&pgis=1 (accessed October 19, 2015).
[28] E. Nam, Y.-H. Kang, D.-J. Son, D. Jung, S.-J. Hong, Y.S. Kim, Electrical and surface properties of indium tin oxide (ITO) films by pulsed DC magnetron sputtering for organic light emitting diode as anode material, Surf. Coatings Technol. 205 (2010) S129–S132. doi:10.1016/j.surfcoat.2010.06.060.
[29] R.N. Chauhan, R.S. Anand, J. Kumar, Structural, electrical and optical properties of radio frequency sputtered indium tin oxide thin films modified by annealing in silicon oil and vacuum, Thin Solid Films. 556 (2014) 253–259. doi:10.1016/j.tsf.2014.02.023.
[30] SnS_2 PDF-2 card no. 00-001-1010
[31] SnS PDF-2 card no. 00-014-0620
[32] Sn_2S_3 PDF-2 card no. 00-014-0619
[33] H.R. Chandrasekhar, R.G. Humphreys, U. Zwick, M. Cardona, Infrared and Raman spectra of

the IV-VI compounds SnS and SnSe, Phys. Rev. B. 15 (1977) 2177–2183. doi:10.1103/PhysRevB.15.2177.
[34] H.R. Chandrasekhar, D.G. Mead, Long-wavelength phonons in mixed-valence semiconductor Sn II Sn IV S 3, Phys. Rev. B. 19 (1979) 932–937. doi:10.1103/PhysRevB.19.932.
[35] P.M. Nikolic, P. Mihajlovic, B. Lavrencic, Splitting and coupling of lattice modes in the layer compound SnS, J. Phys. C Solid State Phys. 10 (1977) L289–L292. doi:10.1088/0022-3719/10/11/003.
[36] A.J. Smith, P.E. Meek, W.Y. Liang, Raman scattering studies of SnS_2 and $SnSe_2$, J. Phys. C Solid State Phys. 10 (1977) 1321–1323. doi:10.1088/0022-3719/10/8/035.
[37] P. Jain, P. Arun, Influence of grain size on the band-gap of annealed SnS thin films, Thin Solid Films. 548 (2013) 241–246. doi:10.1016/j.tsf.2013.09.089.
[38] K.A. Alim, V.A. Fonoberov, A.A. Balandin, Origin of the optical phonon frequency shifts in ZnO quantum dots, Appl. Phys. Lett. 86 (2005) 053103. doi:10.1063/1.1861509.
[39] R.C. Teixeira, I. Doi, M.B.P. Zakia, J.A. Diniz, J.W. Swart, Micro-Raman stress characterization of polycrystalline silicon films grown at high temperature, Mater. Sci. Eng. B. 112 (2004) 160–164. doi:10.1016/j.mseb.2004.05.025.
[40] Q. Zai-Xiang, S. Yun, H. Wei-Yu, L. Wei, H. Qing, L. Chang-Jian, Raman scattering of polycrystalline GaSb thin films grown by the co-evaporation process, Chinese Phys. B. 18 (2009) 2012–2015. doi:10.1088/1674-1056/18/5/047.
[41] C. Julien, H.S. Mavi, K.P. Jain, M. Balkanski, C. Perez-Vicente, J. Morales, Resonant Raman scattering studies of SnS_2 crystals, Mater. Sci. Eng. B, Solid-State Mater. Adv. Technol. 23 (1994) 98–104. http://cat.inist.fr/?aModele=afficheN&cpsidt=4033974 (accessed December 25, 2015).
[42] A.K. Garg, Concentration dependent vibrational mode behaviour in the mixed crystal system SnS_xSe_{2-x}, J. Mol. Struct. 247 (1991) 47–60. doi:10.1016/0022-2860(91)87062-M.
[43] D.G. Mead, J.C. Irwin, Raman spectra of SnS_2 and $SnSe_2$, Solid State Commun. 20 (1976) 885–887. doi:10.1016/0038-1098(76)91297-7.
[44] L.S. Price, I.P. Parkin, A.M.E. Hardy, R.J.H. Clark, T.G. Hibbert, K.C. Molloy, Atmospheric Pressure Chemical Vapor Deposition of Tin Sulfides (SnS, Sn_2S_3, and SnS_2) on Glass, Chem. Mater. 11 (1999) 1792–1799. doi:10.1021/cm990005z.
[45] B. Thangaraju, P. Kaliannan, Spray Pyrolytic Deposition and Characterization of SnS and SnS_2 Thin Films, J. Phys. D - Appl. Phys. 33 (2000) 1054–1059. doi:10.1088/0022-3727/33/9/304.
[46] A.K. Abass, K.J. Majeid, H.A. Jassim, W.A. Murad, Optical properties of chemically deposited tin disulfide coatings, Solid State Commun. 57 (1986) 805–808. doi:10.1016/0038-1098(86)90180-8.
[47] A. Sanchez-Juarez, A. Ortiz, Effects of precursor concentration on the optical and electrical properties of Sn_XS_Y thin films prepared by plasma-enhanced chemical vapour deposition, Semicond. Sci. Technol. 17 (2002) 931–937. doi:Pii S0268-1242(02)32822-0\nDoi 10.1088/0268-1242/17/9/305.
[48] K.T. Ramakrishna Reddy, G. Sreedevi, K. Ramya, R. Miles, Physical properties of Nano-crystalline SnS_2 layers grown by chemical bath deposition, Energy Procedia. (2012). http://nrl.northumbria.ac.uk/8186/ (accessed February 4, 2016).
[49] R.H. Williams, R.B. Murray, D.W. Govan, J.M. Thomas, E.L. Evans, Band structure and photoemission studies of SnS_2 and $SnSe_2$. I. Experimental, J. Phys. C Solid State Phys. 6 (1973) 3631–3642. doi:10.1088/0022-3719/6/24/022.
[50] S.G. Patil, R.H. Tredgold, Electrical and photoconductive properties of SnS_2 crystals, J. Phys. D. Appl. Phys. 4 (2002) 718–722. doi:10.1088/0022-3727/4/5/312.

[51] J. George, C.K.V. Kumari, Electrical characterization of tin disulphide crystals, Solid State Commun. 49 (1984) 103–106.
[52] M. Devika, N.K. Reddy, F. Patolsky, K.R. Gunasekhar, Ohmic contacts to SnS films: Selection and estimation of thermal stability, J. Appl. Phys. 104 (2008) 124503. doi:10.1063/1.3041622.
[53] B.L. Sharma, Chapter 1 Ohmic Contacts to III-V Compound Semiconductors, Semicond. Semimetals. 15 (1981) 1–38. doi:10.1016/S0080-8784(08)60284-7.
[54] C.D. Lokhande, A chemical method for tin disulphide thin film deposition, J. Phys. D. Appl. Phys. 23 (1990) 1703–1705. doi:10.1088/0022-3727/23/12/032.
[55] K. Vijayakumar, C. Sanjeeviraja, M. Jayachandran, L. Amalraj, Characterization of Tin disulphide thin films prepared at different substrate temperature using spray pyrolysis technique, J. Mater. Sci. Mater. Electron. 22 (2011) 929–935. doi:10.1007/s10854-010-0239-z.

Table 1. Positions and possible mode assignments of the observed Raman peaks.

Phase	Crystal symmetry	Modes frequencies, cm^{-1}						
		Reference data [33,34,36]	Non-irradiated		Irradiated I_1=8.5 MW/cm^2		Irradiated I_2=11.5 MW/cm^2	
			excitation		excitation		excitation	
			green	IR	green	IR	green	IR
SnS_2	A_{1g}	315	314.7	314.5	314.7	314.5	314.7	314.5
	E_g	205	204	204	-	-	-	-
Sn_2S_3	A_g	308±2	-	-	-	309	310	309
		236±2	-	-	236	-	236	-
		154±2	-	-	-	154	-	154
		~ 90	-	-	88	88	88	88
SnS	A_g	218±2	-	-	220	222	220	221
		192±2	-	-	189	184	189	184
		95±2	-	-	95	95	95	95
	B_{3g}	164±2	-	-	-	-	162	-
	B_{2g}	290±4	-	-	-	288	-	288
		160	-	-	-		-	
		85±2	-	-	-		-	

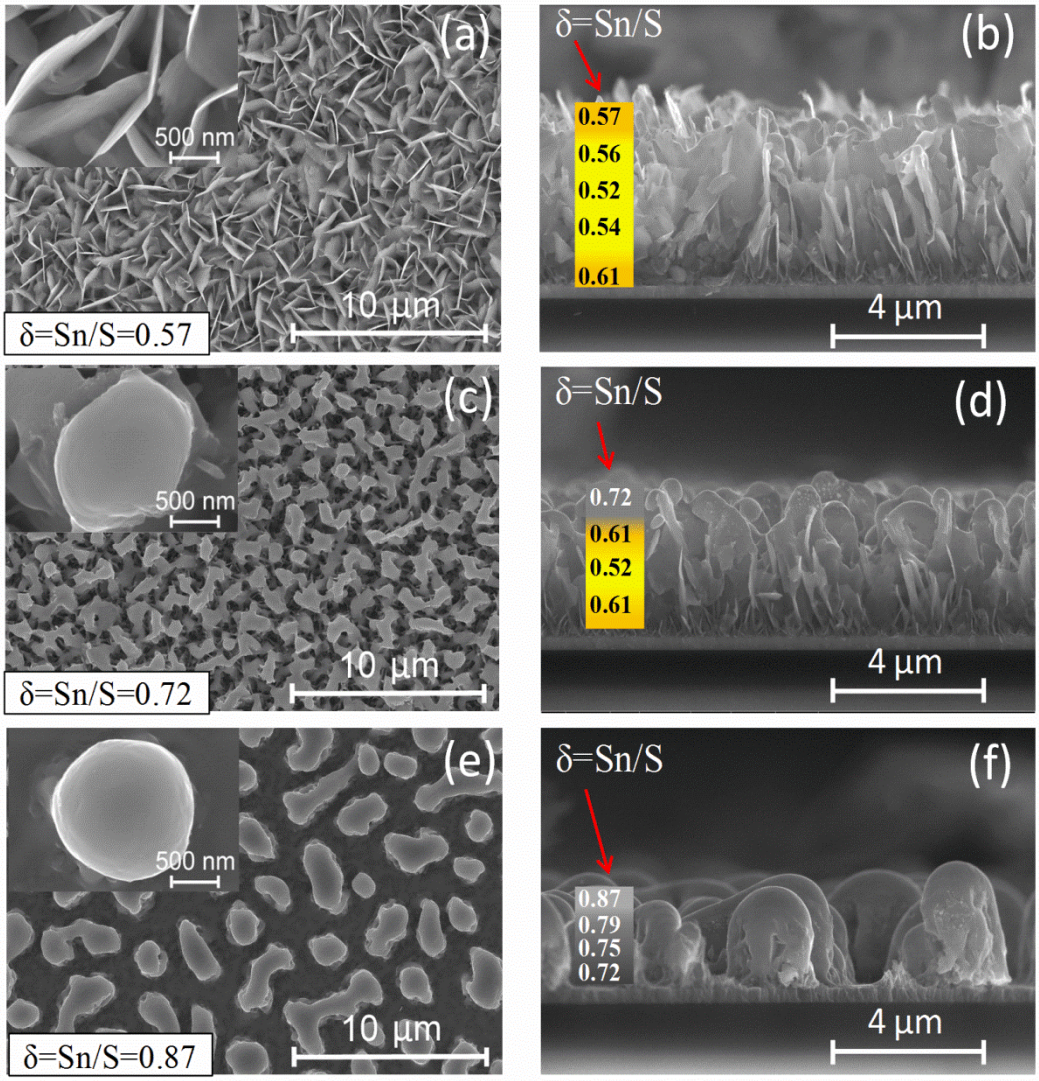

Fig.1 FESEM images of surface and cross section of the samples: non-irradiated sample (a)-surface, (b) - cross section; sample annealed with laser of I_1=8.5 MW/cm^2 intensity (c)-surface, (d)- cross section; sample annealed with laser of I_2=11.5 MW/cm^2 intensity (e)-surface, (f)- cross section. Results of EDS study of chemical composition (δ=Sn/S) for the surface are presented on insets and for the cross section on rectangles (position of δ values on images of cross section correspond to a spot of measurement).

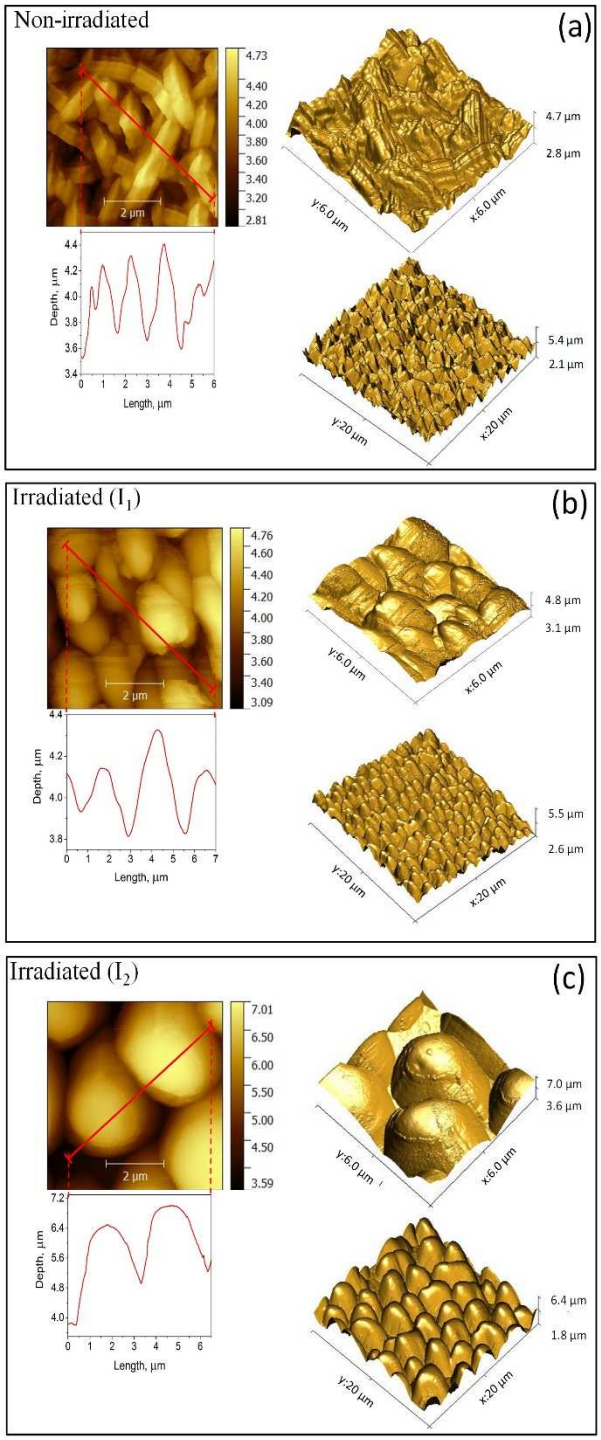

Fig.2 AFM 3-D and surface images with their profile (along red line on the surface): non-irradiated sample (a); samples annealed with a laser of I_1=8.5 MW/cm^2 (b) and I_2=11.5 MW/cm^2 (d) intensities.

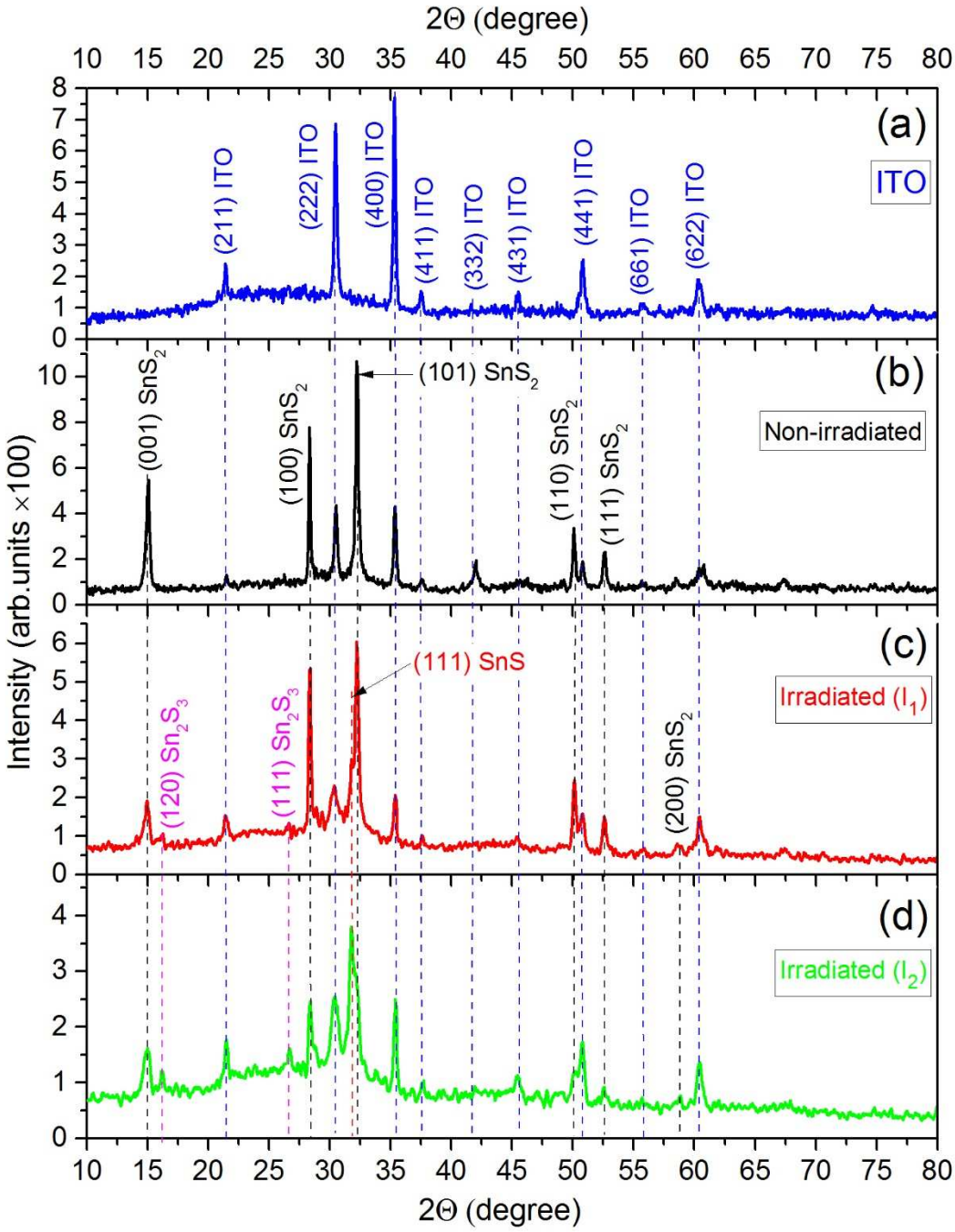

Fig. 3. XRD patterns of the samples: ITO-coated glass substrate (a); non-irradiated sample (b); samples annealed with laser of I_1=8.5 MW/cm^2 (c) and I_2=11.5 MW/cm^2 (d) intensities.

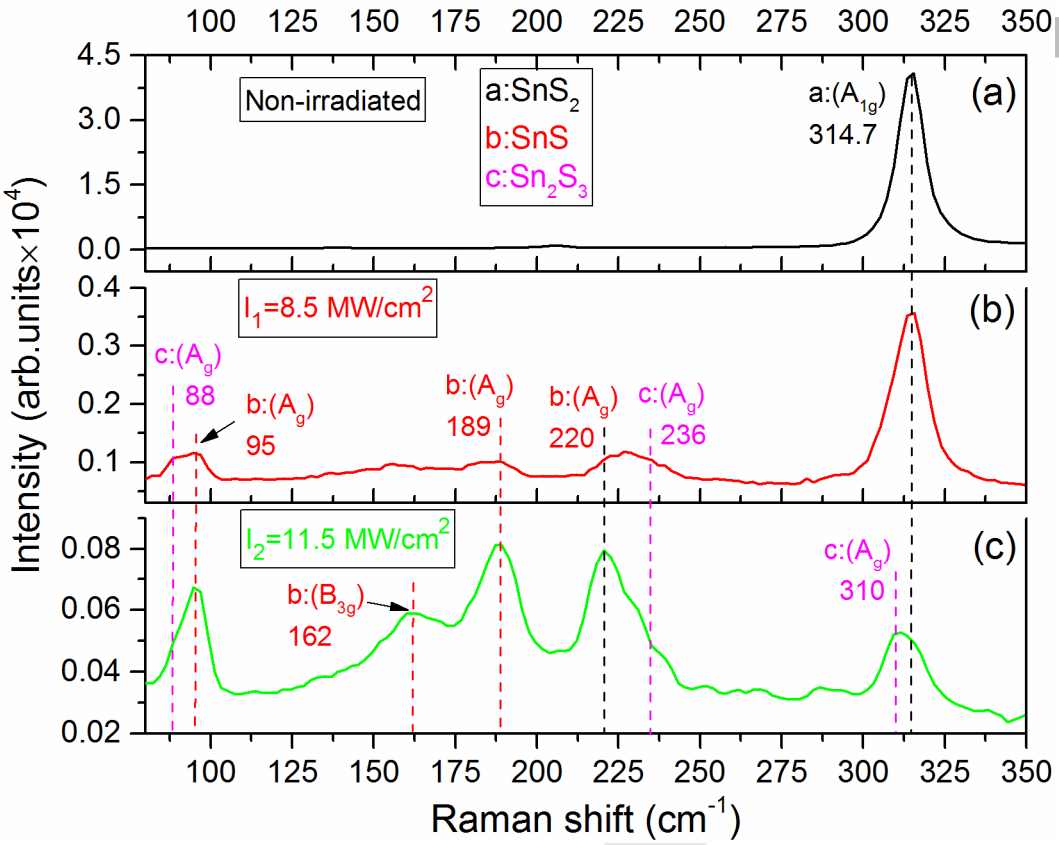

Fig. 4. Raman spectra of the samples obtained with excitation by the green Ar laser λ=514 nm: non-irradiated sample (a); samples annealed with a laser of I_1=8.5 MW/cm^2 (b) and I_2=11.5 MW/cm^2 (c) intensities.

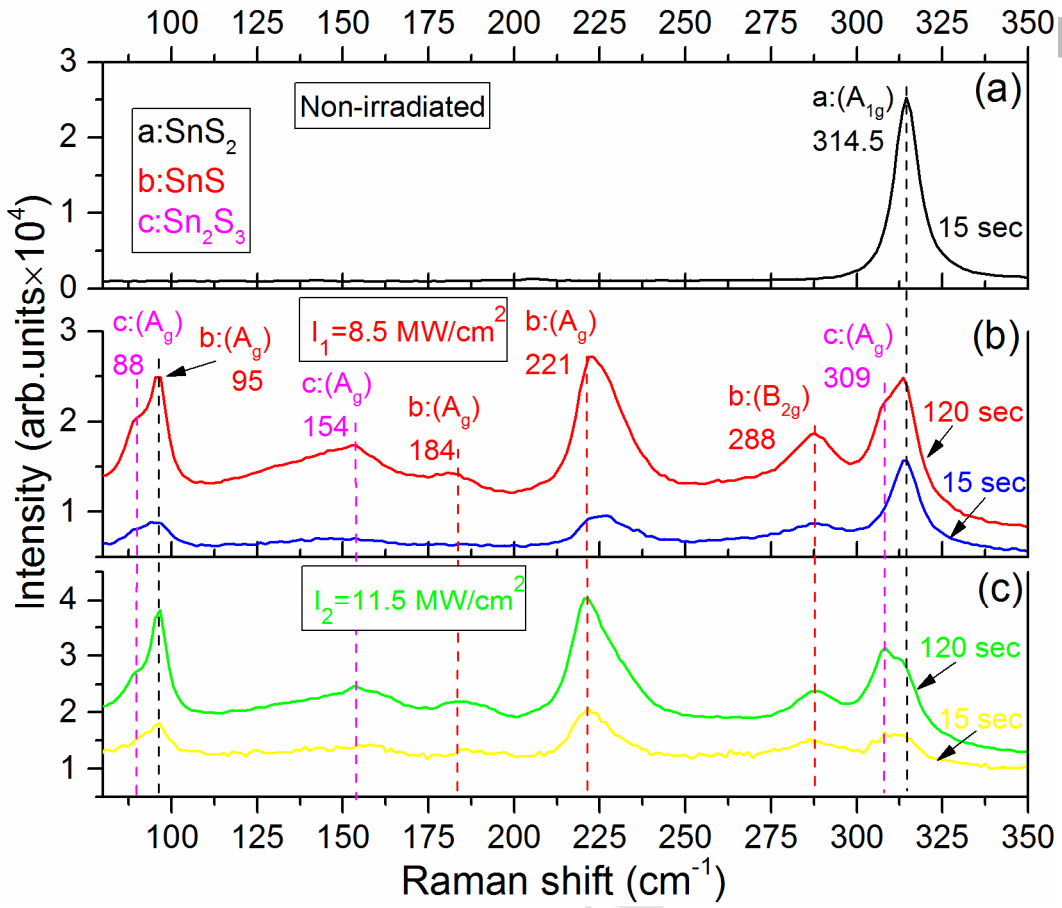

Fig. 5 Raman spectra of the samples obtained with excitation by the IR laser λ=785 nm and different exposure time of 10 or 30 sec: non-irradiated sample (a); samples annealed with a laser of I_1=8.5 MW/cm^2 (b) and I_2=11.5 MW/cm^2 (c) intensities.

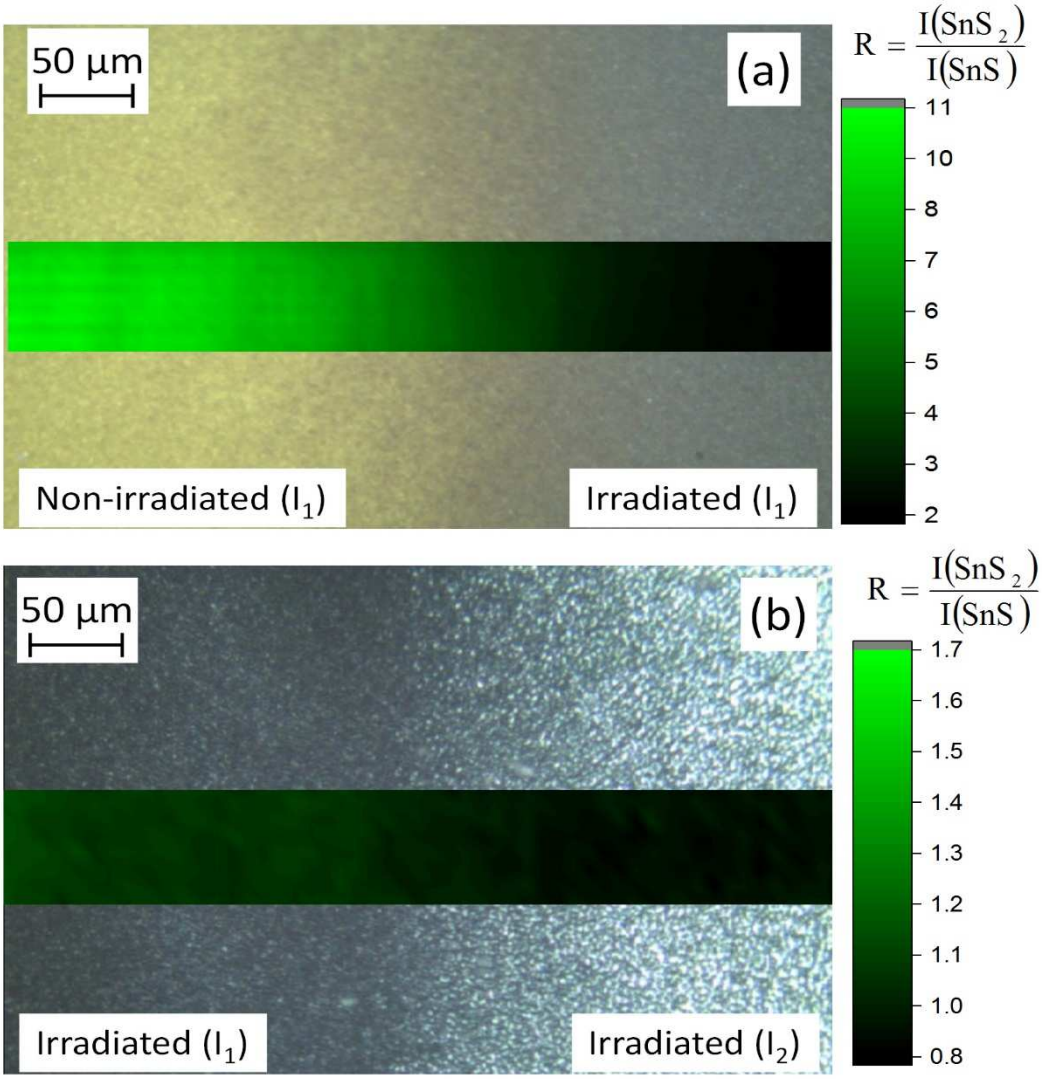

Fig. 6 Raman spectra of the samples obtained with excitation by the IR laser λ=785 nm: non-irradiated sample (a); samples annealed with a laser of I_1=8.5 MW/cm^2 (b) and I_2=11.5 MW/cm^2 (c) intensities.

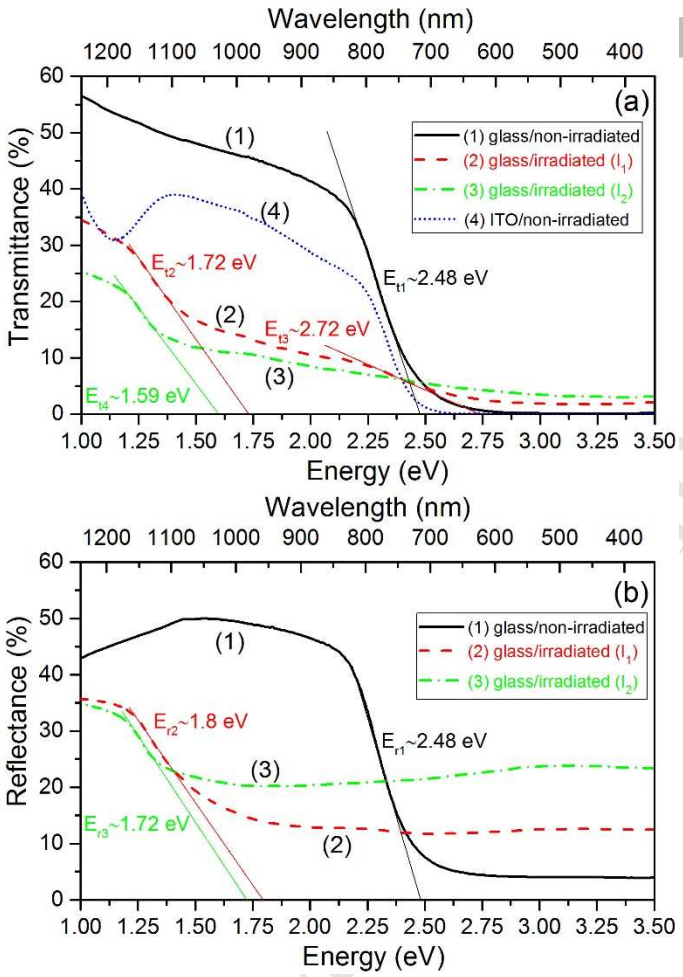

Fig. 7. The reflectance (a) and transmittance (b) spectra of: non-irradiated sample (1); samples irradiated with a laser of I_1=8.5 MW/cm^2 (2) and I_2=11.5 MW/cm^2 (3) intensities.

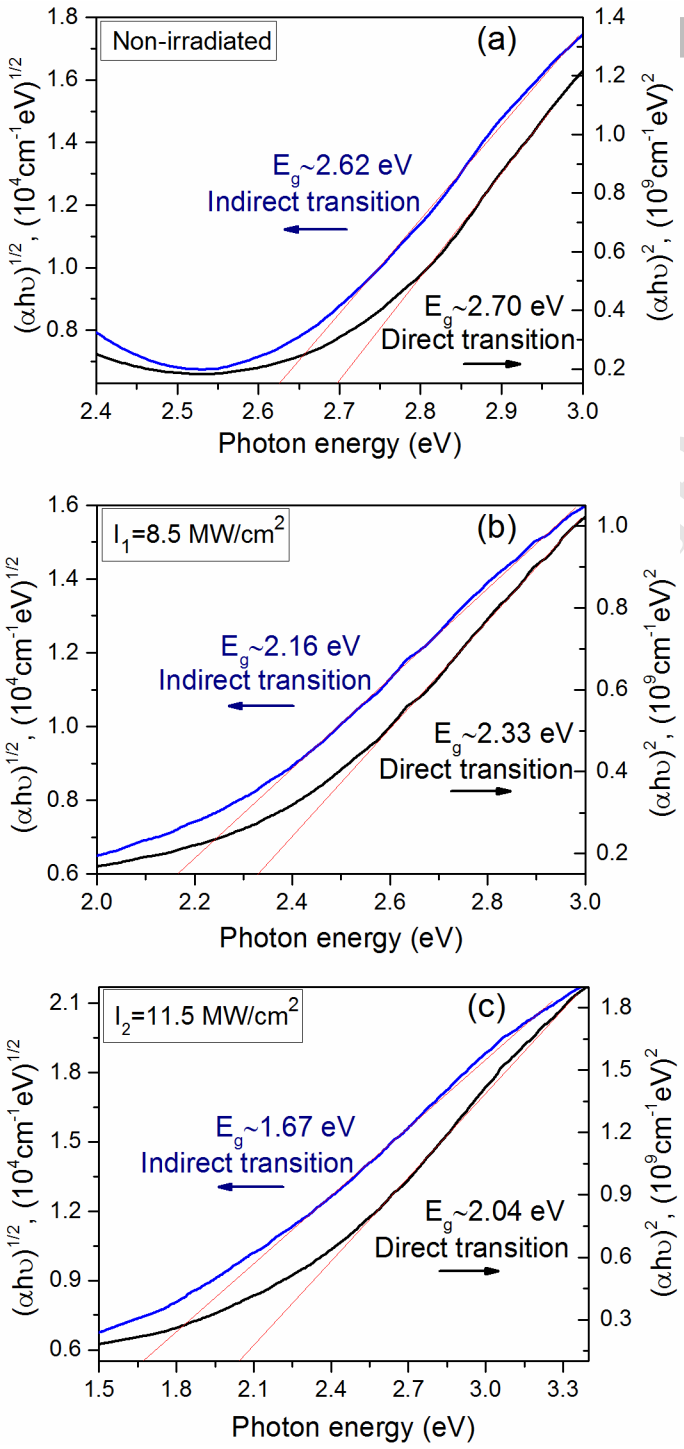

Fig. 8. The energy gap determination for: non-irradiated sample (a); samples irradiated with a laser of I_1=8.5 MW/cm^2 (b) and I_2=11.5 MW/cm^2 (c) intensities.

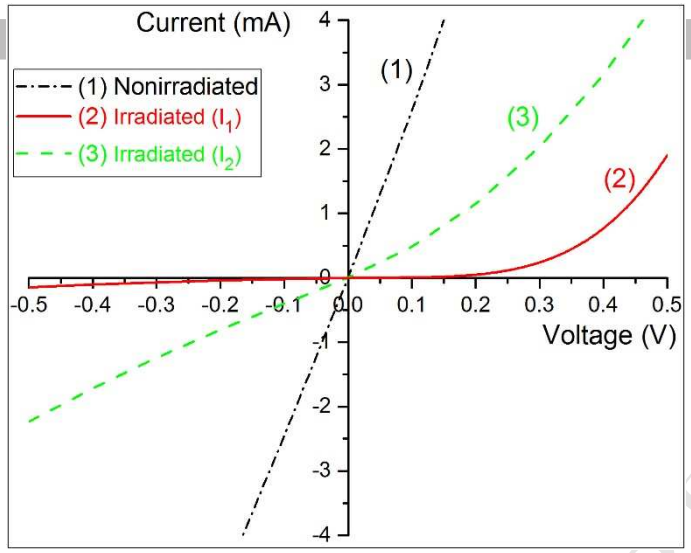

Fig. 9. The current-voltage dependencies of the ITO/Sn_xS_y/Al samples: nonirradiated (1); samples irradiated with a laser of I_1=8.5 MW/cm^2 (2) and I_2=11.5 MW/cm^2 (3) intensities.

HIGHLIGHTS

- The SnS_2 single-phase thin films were obtained by the close-spaced vacuum sublimation method.
- Laser irradiation of the SnS_2 films provides evaporation of sulphur and hence phase transition to the SnS phase.
- Irradiation of the sample leads to the smoothing of the surface due to the melting accompanied by the agglomeration of the grains into the islands.
- The electrical measurements of the irradiated samples show diode behavior of the current-voltage dependencies that is evidence of formation of the two-layer n-SnS_2/p-SnS heterojunction structure.